Synthesis and Cleavage Reactions of Metal−Metal-Bonded $[Mo_2(S_2CNR_2)_6](OTf)_2$, a Source of the Tris(dithiocarbamato)molybdenum(IV) Fragment

Sean B. Seymore[†] and Seth N. Brown*

Department of Chemistry and Biochemistry, 251 Nieuwland Science Hall, University of Notre Dame, Notre Dame, Indiana 46556-5670

Received June 25, 2001

Halide abstraction from the chlorotris(dialkyldithiocarbamato)molybdenum(IV) complexes $MoCl(S_2CNR_2)_3$ (R = Et, Me) with silver triflate produces the diamagnetic dimeric complexes $[Mo_2(S_2CNR_2)_6](OTf)_2$ in good yield. The crystallographically determined structure of the diethyldithiocarbamato complex indicates that the dimer consists of two pentagonal bipyramids sharing an axial edge, with a Mo−Mo separation (2.8462(8) Å) indicative of a metal−metal bond. A qualitative analysis of the bonding indicates that this bond is of order 2 and consists of one normal σ bond and one relatively weak "skewed π" interaction. The dimers $[Mo_2(S_2CNR_2)_6](OTf)_2$ react with a variety of reagents to give monomeric seven-coordinate complexes, including the new cationic molybdenum(IV) complex $[Mo(PMe_2Ph)(S_2CNEt_2)_3](OTf)$, which has been structurally characterized. Kinetic studies of the reaction of $[Mo_2(S_2CNEt_2)_6](OTf)_2$ with halides indicate the presence of competing dissociative and associative substitution pathways, although neutral donors may react by different mechanisms.

Introduction

The coordination chemistry of molybdenum has received considerable attention due to the occurrence of this metal in a number of important biological systems.[1,2] There has been particular interest in sulfur-rich Mo complexes, which are used to form reactive clusters[3] and to mimic the metal−ligand environment found in molybdoenzymes.[4] Pioneering work done by Chatt and co-workers employed the tris(dialkyldithiocarbamato)molybdenum unit, $\{Mo(S_2CNR_2)_3\}$, as the core for many model complexes, including $Mo(N_2COPh)(S_2CNR_2)_3$ (**1**),[5] $MoCl(S_2CNR_2)_3$ (**2**),[5] and $MoN(S_2CNR_2)_3$ (**3**).[6]

Given the utility and stability of the molybdenum tris(dithiocarbamate) core, we sought a convenient source of the molybdenum(IV) fragment $[Mo(S_2CNR_2)_3]^+$. Here we report that this cation appears to be unstable as a monomer, instead dimerizing to form metal−metal-bonded dimers $[Mo_2(S_2CNR_2)_6](OTf)_2$ (**4**). Metal−metal bonding is a staple of molybdenum chemistry and has been very extensively studied.[7] However, the seven-coordinate geometries of the molybdenum atoms in **4** create an unusual form of multiple bonding in this complex, with a formally double, but very long, molybdenum−molybdenum bond. The strength of the metal−metal interaction helps to hold the dimer together in solution, but **4** is cleaved by a variety of reagents under relatively mild conditions and thus does serve as a source of the $[Mo(S_2CNR_2)_3]^+$ fragment.

Experimental Section

Unless otherwise noted, all procedures were carried out on the bench top. Acetonitrile, chloroform, and methylene chloride were dried over 4 Å molecular sieves, followed by CaH_2. Acetone was dried over 4 Å molecular sieves. Dry ether was vacuum transferred from sodium benzophenone ketyl. $MoO_2(S_2CNR_2)_2$ complexes [R = Et (**a** series), Me (**b** series)] were prepared using a literature procedure.[8] $Mo(N_2COPh)(S_2CNR_2)_3$ (**1**) and $MoCl(S_2CNR_2)_3$ (**2**) were prepared using the procedures outlined in a short communication;[5] details and ^1H NMR spectral data for the compounds are given below. $MoN(S_2CNR_2)_3$ was prepared using a literature method.[6] All other reagents were commercially available and used without further purification.

NMR spectra were measured on a General Electric GN-300 or a Varian-300 FT-NMR spectrometer. Chemical shifts for ^1H and $^{13}C\{^1H\}$ spectra are reported in ppm referenced to TMS. Those for ^{19}F and $^{31}P\{^1H\}$ spectra are reported in ppm referenced to external trifluoroacetic and phosphoric acid, respectively. Infrared spectra were recorded as evaporated films on KBr plates on a Perkin-Elmer Paragon 1000 FT-IR spectrometer. UV−visible data were collected on a Beckman DU-7500 diode-array spectrophotometer (300−800 nm) equipped with a multicell transport block or a Perkin-Elmer UV/vis/NIR Lambda 19 spectrophotometer (300−3000 nm). Mass spectra were obtained on a JEOL JMS-AX 505HA mass spectrometer using the FAB ionization

[†] Current address: Department of Chemistry, Rose-Hulman Institute of Technology, 5500 Wabash Avenue, Terre Haute, IN 47803.

(1) (a) Bolin, J. T.; Campobasso, N.; Muchmore, S. W.; Morgan, T. V.; Mortenson, L. E. In *Molybdenum Enzymes, Cofactors, and Model Systems*; Stiefel, E. I., Coucouvanis, D., Newton, W. E., Eds.; ACS Symp. Series 535; American Chemical Society: Washington, DC, 1993; pp 186−195. (b) Rajagopalan, K. In *Molybdenum and Molybdenum Containing Enzymes*; Coughlan, M., Ed.; Pergamon: Oxford, U.K., 1980; pp 241−272.

(2) (a) Hille, R. *Chem. Rev.* **1996**, *96*, 2757−2816. (b) Holm, R. H. *Chem. Rev.* **1987**, *87*, 1401−1449.

(3) (a) Mayor-Lopez, M. J.; Weber, J.; Hegetschweiler, K.; Meienberger, M. D.; Joho, F.; Leoni, S.; Nesper, R.; Reiss, G. J.; Frank, W.; Kolesov, B. A.; Fedin, V. P.; Fedorov, V. E. *Inorg. Chem.* **1998**, *37*, 2633−2644. (b) Dance, I.; Fisher, K. *Prog. Inorg. Chem.* **1994**, *41*, 637−803. (c) Meienberger, M. D.; Hegetschweiler, K.; Ruegger, H.; Gramlich, V. *Inorg. Chim. Acta* **1993**, *213*, 157−169. (d) Shibahara, T. *Coord. Chem. Rev.* **1993**, *123*, 73−147. (e) Zimmermann, H.; Hegetschweiler, K.; Keller, T.; Gramlich, V.; Schmalle, H. W.; Petter, W.; Schneider, W. *Inorg. Chem.* **1991**, *30*, 4336−4341.

(4) See for example: (a) Thapper, A.; Lorber, C.; Fryxelius, J.; Behrens, A.; Norlander, E. *J. Inorg. Biochem.* **2000**, *79*, 67−74. (b) Smith, P. D.; Millar, A. J.; Young, C. G.; Ghosh, A.; Basu, P. *J. Am. Chem. Soc.* **2000**, *122*, 9298−9299. (c) Smith, P. D.; Slizys, D. A.; George, G. N.; Young, C. G. *J. Am. Chem. Soc.* **2000**, *122*, 2946−2947. (d) Mader, M. L.; Carducci, M. D.; Enemark, J. H. *Inorg. Chem.* **2000**, *39*, 525−531.

(5) Bishop, M. W.; Chatt, J.; Dilworth, J. R. *J. Organomet. Chem.* **1974**, *73*, C59−C60.

(6) Chatt, J.; Dilworth, J. R. *J. Indian Chem. Soc.* **1977**, *54*, 13−18.

(7) Cotton, F. A.; Walton, R. A. *Multpile Bonds Between Metal Atoms*, 2nd ed.; Clarendon: Oxford, U.K., 1993; pp 682−719.

(8) Moore, F. W.; Larson, M. L. D. *Inorg. Chem.* **1967**, *6*, 998−1003.

10.1021/ic010673y CCC: $20.00 © 2001 American Chemical Society
Published on Web 11/17/2001

mode and 3-nitrobenzyl alcohol as a matrix. In all cases, observed intensities were in satisfactory agreement with calculated isotopic distributions. Elemental analyses were performed by M-H-W Laboratories (Phoenix, AZ) or Canadian Microanalytical Services, Ltd. (Vancouver, BC, Canada).

$Mo(N_2COPh)(S_2CNEt_2)_3$ (1a).[5] To a 250-mL round-bottom flask were added a magnetic stirbar, $MoO_2(S_2CNEt_2)_2$ (2.53 g, 5.96 mmol), $NaS_2CNEt_2{\cdot}3H_2O$ (Aldrich, 1.60 g, 7.10 mmol), $PhCONHNH_2$ (Aldrich, 0.88 g, 6.46 mmol), and absolute MeOH (100 mL). After stirring of the mixture at reflux for 3 h, the orange product was collected by filtration, washed with two 10 mL aliquots of absolute MeOH, and air-dried. Yield: 3.17 g (79%). ^{1}H NMR ($CDCl_3$): δ 1.27 (m, 18H, CH_3); 3.77 (m, 12H, CH_2); 7.28 (t, J = 8 Hz, 2H, meta); 7.38 (t, J = 8 Hz, 1H, para); 8.03 (d, J = 7 Hz, 2H, ortho).

$Mo(N_2COPh)(S_2CNMe_2)_3$ (1b).[5] Following the procedure for **1a**, $MoO_2(S_2CNMe_2)_2$ (2.72 g, 7.38 mmol) yielded 0.70 g (16%) of orange product. ^{1}H NMR (CD_2Cl_2): δ 3.26 (s, 3H, CH_3), 3.28 (s, 6H, CH_3), 3.32 (s, 6H, CH_3), 3.39 (s, 3H, CH_3); 7.32 (t, J = 8 Hz, 2H, meta); 7.44 (t, J = 8 Hz, 1H, para); 8.03 (d, J = 7 Hz, 2H, ortho).

$MoCl(S_2CNEt_2)_3$ (2a).[5] To a 250-mL round-bottom flask were added a magnetic stirbar, **1a** (2.05 g, 0.304 mmol), and absolute methanol (100 mL). Gaseous HCl, generated from H_2SO_4 and saturated brine and dried by passage through H_2SO_4, was vigorously bubbled through the orange suspension for 15 min. Heat was generated, and the mixture turned forest green. The flask was quickly affixed to a vacuum line, and the volume was reduced to 30 mL. The resulting green solid was collected on a frit under vacuum and washed with 10 mL of freshly distilled CH_3OH. The product was dried under vacuum and stored in the drybox. Yield: 1.09 g (63%). ^{1}H NMR (CD_2Cl_2): δ 1.33 (s, 18H, CH_3); 25.29 (br, 12H, CH_2). UV−vis (CH_2Cl_2) [λ, nm (ϵ, M^{-1} cm^{-1})]: 363 (7200), 406 (sh, 2600), 592 (80).

$MoCl(S_2CNMe_2)_3$ (2b).[5] Following the procedure above, **1b** (1.00 g, 1.70 mmol) furnished the green product **2b** (0.58 g, 68%). ^{1}H NMR (CD_2Cl_2): δ 38.41 (br s, 18H, CH_3).

$[Mo_2(S_2CNEt_2)_6](OTf)_2$ (4a). In the drybox, **2a** (1.09 g, 1.89 mmol), AgOTf (Aldrich, 540 mg, 2.10 mmol), and a magnetic stirbar were added to a 100-mL round-bottom flask. The flask was attached to a swivel frit, which was then affixed to a vacuum line. Dry CH_2Cl_2 (30 mL) was added by vacuum transfer, and the solution was stirred in the dark for 3 h. The insoluble material was removed by filtration, and ether (30 mL) was condensed on the resulting brown solution. The next day, the brown solid was collected by filtration and taken into the drybox. Yield: 1.07 g (81%). Alternatively, TlOTf can be substituted for AgOTf in this procedure and used to prepare the product in similar yields. ^{1}H NMR (CD_2Cl_2): δ 1.34 (m, 36H, CH_3); 3.79 (m, 24H, CH_2). ^{13}C{^{1}H} NMR (CD_2Cl_2): δ 12.71, 12.82, 12.85, 12.89, 13.31, 14.08 (CH_2CH_3); 44.94, 45.34, 46.25, 46.37, 46.53, 46.77 (CH_2CH_3); 196.12, 196.98 (CS_2). ^{19}F{^{1}H} NMR (CD_2Cl_2): δ −1.03 (s, 6F, CF_3). IR (cm^{-1}): 1523 (vs), 1460 (m), 1443 (s), 1383 (m), 1357 (m), 1273 (vs, ν_{SO_3}), 1223 (m), 1205 (m), 1152 (s, ν_{CF_3}), 1096 (w), 1076 (m), 1031 (vs, ν_{SO_3}), 970 (w), 916 (w), 850 (m), 780 (2), 754 (w), 638 (vs). FABMS: m/e 1081, $(M - H^+)^+$. UV−vis (CH_2Cl_2) [λ, nm (ϵ, M^{-1} cm^{-1})]: 398 (6300), 466 (4800), 517 (sh, 2500), 582 (sh, 1400), 817 (1200). Anal. Calcd for $C_{32}H_{60}F_6Mo_2N_6O_6S_{14}$: C, 27.86; H, 4.38; N, 6.09. Found: C, 27.47; H, 4.41; N, 5.86.

$[Mo_2(S_2CNMe_2)_6](OTf)_2$ (4b). Following the procedure above, **2b** (479.0 mg, 1.01 mmol) furnished 419.3 mg of $[Mo_2(S_2CNMe_2)_6](OTf)_2$ (**4b**) as a brown solid (68%). ^{1}H NMR (acetone-d_6): δ 3.41 (s, 6H, CH_3), 3.42 (s, 6H, CH_3), 3.49 (s, 6H, CH_3), 3.51 (s, 6H, CH_3), 3.53 (s, 6H, CH_3), 3.74 (s, 6H, CH_3). ^{13}C{^{1}H} NMR (CD_2Cl_2): δ 39.25, 39.73, 40.55, 40.90, 41.05, 42.01 (CH_3); 196.92 (CS_2). ^{19}F{^{1}H} NMR (CD_2Cl_2): δ 0.34 (s, 6F, CF_3). IR (cm^{-1}): 1549 (vs), 1446 (m), 1401 (vs), 1261 (vs, ν_{SO_3}), 1224 (s), 1155 (vs, ν_{CF_3}), 1030 (vs, ν_{SO_3}), 991 (m), 638 (vs). FABMS: m/e 913, $(M - H^+)^+$. Anal. Calcd for $C_{20}H_{36}F_6Mo_2N_6O_6S_{14}$: C, 19.83; H, 3.00; N, 6.94. Found: C, 19.64; H, 3.17; N, 6.69.

$[(Et_2NCS_2)_3Mo(\mu\text{-}N)Mo(S_2CNEt_2)_3]OTf$ (5a) was generated in solution. In a typical experiment $(Et_2NCS_2)_3MoN$ (**3a**, 6.6 mg, 11.9 μmol) and **4a** (10.5 mg, 7.6 μmol) were dissolved in CD_2Cl_2 (0.5 mL) in the drybox. The solution was added to a screw-cap NMR tube and monitored by ^{1}H NMR spectroscopy. The resulting equilibrium mixture, established within minutes, includes the new product. ^{1}H NMR (CD_2Cl_2): δ 1.52 (br, 36H, CH_3); 17.94 (br, 24H, CH_2). FABMS: m/e 1095, $(M - H)^+$. The complex **$[(Me_2NCS_2)_3Mo(\mu\text{-}N)Mo(S_2CNMe_2)_3]OTf$ (5b)** was prepared analogously. ^{1}H NMR (CD_2Cl_2): δ 27.88 (br, 36H, CH_3). The mixed complex **$[(Me_2NCS_2)_3Mo(\mu\text{-}N)Mo(S_2CNEt_2)_3]OTf$ (5c)** can be obtained by mixing **3a** and **4b**, or **3b** and **4a**, in CD_2Cl_2. The resulting equilibrium mixture includes **5a**,**b** and the new product. ^{1}H NMR (CD_2Cl_2): δ 1.55 (br, 18H, CH_2CH_3), 18.90 (br, 12H, CH_2-CH_3), 26.29 (br, 18H, NCH_3).

$Mo(N_3)(S_2CNEt_2)_3$ was generated in solution. In the drybox an NMR tube with a Teflon-lined screw cap was charged with **4a** (5.9 mg, 4.3 μmol), NaN_3 (Fisher, 6.0 mg, 0.09 mmol), and CD_3CN (0.5 mL). Reaction progress was monitored by ^{1}H NMR spectroscopy for 24 h. During this time period the intermediate $Mo(N_3)(S_2CNEt_2)_3$ was observed. ^{1}H NMR (CD_3CN): δ 1.52 (br, 18H, CH_3), 17.71 (br, 12H, CH_2CH_3). Immersion of the tube in a 60 °C oil bath for 1 h led to the quantitative formation of **3a**.

$[Mo(PMe_2Ph)(S_2CNEt_2)_3]OTf$ ([6]OTf). In the drybox, **4a** (243 mg, 0.176 mmol), PMe_2Ph (Strem, 145 mg, 1.10 mmol), and a magnetic stirbar were added to a 50-mL round-bottom flask. The flask was attached to the vacuum line. Dry acetone (20 mL) was added by vacuum transfer, and the solution was stirred in vacuo for 2 d. The volume was reduced to 15 mL, and ether (20 mL) was condensed on the reddish-brown solution. The next day, the reaction mixture was taken into the drybox, and the red crystals were filtered out and washed with ether. Yield: 113 mg (39%). ^{1}H NMR ($CDCl_3$): δ −18.15 (br, 6H, PCH_3), 1.69 (s, 18H, CH_2CH_3), 7.43 (s, 1H, para), 10.74 (s, 2H, meta), 14.90 (br, 2H, ortho), 35.39 (s, 12H, CH_2CH$_3$). IR (cm^{-1}): 1519 (s), 1460 (m), 1441 (m), 1383 (m), 1357 (m), 1274 (vs, ν_{SO_3}), 1224 (m), 1205 (m), 1152 (m, ν_{CF_3}), 1097 (w), 1076 (m), 1000 (w), 935 (m), 913 (w), 850 (w), 781 (w), 749 (w), 696 (w), 638 (s). UV−vis (CH_2Cl_2) [λ, nm (ϵ, M^{-1} cm^{-1})]: 418 (5400). Anal. Calcd for $C_{24}H_{41}F_3MoN_3O_3PS_7$: C, 34.82; H, 4.99; N, 5.08. Found: C, 35.00; H, 4.24; N, 5.14.

$[Mo(PPh_3)(S_2CNEt_2)_3]OTf$ was generated in solution by addition of PPh_3 (2 equiv) to a solution of **4a** in acetone-d_6 or CD_2Cl_2. ^{1}H NMR (acetone-d_6): δ 1.49 (br, 18H, CH_3), 7.73 (br, 3H, para), 10.00 (br, 6H, meta), 11.20 (v br, 6H, ortho), 36.87 (br, 12H, CH_2CH$_3$). **$[Mo(NCCD_3)(S_2CNEt_2)_3]OTf$** was generated by dissolving **4a** in CD_3CN. ^{1}H NMR (CD_3CN): δ 1.48 (br, 18H, CH_3), 30.52 (br, 12H, CH_2CH$_3$).

X-ray Structure Determinations of $[Mo_2(S_2CNEt_2)_6](OTf)_2{\cdot}4CHCl_3$ (4a·4CHCl$_3$) and $[Mo(PMe_2Ph)(S_2CNEt_2)_3]OTf$ (6). Crystals of $[Mo_2(S_2CNEt_2)_6](OTf)_2{\cdot}4CHCl_3$ were grown by layering a solution of **4a** in chloroform with diethyl ether (1:3 v/v) and allowing the mixture to stand at −30 °C in the drybox for 2 weeks. A small red plate (0.2 × 0.1 × 0.02 mm) was placed in inert oil and transferred to the tip of a glass fiber in the cold N_2 stream of a Bruker Apex CCD diffractometer (T = −100 °C). Data were reduced, correcting for absorption and decay, using the program SADABS. The crystal was triclinic (space group $P\bar{1}$). The molybdenum atoms were located on a Patterson map, and the remaining non-hydrogen atoms were found on difference Fourier syntheses. Hydrogens were placed in calculated positions. One of the methyl groups (the one attached to C63) was found to be disordered over two positions, which were given equal occupancy in the refinement. Final full-matrix least-squares refinement on F^2 converged at R = 0.0545 for 8439 reflections with $F_o > 4\sigma(F_o)$ and R = 0.0977 for all 13 131 unique reflections (wR_2 = 0.1248, 0.1612, respectively). All calculations used SHELXTL (Bruker Analytical X-ray Systems), with scattering factors and anomalous dispersion terms taken from the literature.[9] Crystallographic data are found in Tables 1−3.

A 0.35 × 0.17 × 0.13 mm red block of $[Mo(PMe_2Ph)(S_2CNEt_2)_3]$-OTf was deposited after slow diffusion of ether into a solution of **6** in acetone. Data collection and reduction were done as described above. The crystal was monoclinic, and its space group was determined to be $P2_1/n$ on the basis of the systematic absences. The molybdenum atoms and the atoms in the first coordination shell were located using direct methods, and remaining nonhydrogen atoms were found on difference Fourier syntheses. Hydrogens were placed in calculated positions. There were two crystallographically independent molecules in the unit cell,

(9) *International Tables of Crystallography*; Kluwer Academic Publishers: Dordrecht, The Netherlands, 1992; Vol. C.

Table 1. Crystallographic Details for $[Mo_2(S_2CNEt_2)_6](OTf)_2 \cdot 4CHCl_3$ (**4a**·$4CHCl_3$) and $[Mo(PMe_2Ph)(S_2CNEt_2)_3]OTf$ (**6**)

	$[Mo_2(S_2CNEt_2)_6](OTf)_2 \cdot 4CHCl_3$ (**4a**·$4CHCl_3$)	$[Mo(PMe_2Ph)(S_2CNEt_2)_3]OTf$ (**6**)
empirical formula	$C_{36}H_{64}Cl_{12}F_6Mo_2N_6O_6S_{14}$	$C_{24}H_{41}F_3MoN_3O_3PS_7$
fw	1857.05	827.93
temp (K)	170	170
λ (Å)	0.710 73 (Mo Kα)	0.710 73 (Mo Kα)
space group	$P\bar{1}$	$P2_1/n$
tot. data collcd	41 562	63 134
no. of indep reflns	13 131	17 026
a (Å)	13.4735(8)	14.544(2)
b (Å)	15.3695(10)	16.716(2)
c (Å)	19.4407(12)	29.745(3)
α (deg)	96.8470(10)	90
β (deg)	92.5940(10)	98.158(2)
γ (deg)	110.6430(10)	90
V (Å^3)	3723.9(4)	7158.3(13)
Z	2	8
calcd ρ (g/cm^3)	1.656	1.536
cryst size (mm)	0.02 × 0.1 × 0.2	0.13 × 0.17 × 0.35
μ (mm^{-1})	1.217	0.866
R indices [$I > 2\sigma(I)$][a]	R1 = 0.0545, wR2 = 0.1248	R1 = 0.0511, wR2 = 0.1149
R indices (all data)[a]	R1 = 0.0977, wR2 = 0.1612	R1 = 0.0838, wR2 = 0.1378

[a] $R1 = \sum||F_o| - |F_c||/\sum|F_o|$; $wR2 = (\sum[w(F_o^2 - F_c^2)^2]/\sum w(F_o^2)^2)^{1/2}$.

Table 2. Selected Bond Lengths (Å) and Angles (deg) for $[Mo_2(S_2CNEt_2)_6](OTf)_2 \cdot 4CHCl_3$ (**4a**·$4CHCl_3$)

Mo1−S11	2.499(2)	Mo2−S51	2.476(2)
Mo1−S12	2.535(2)	Mo2−S52	2.564(2)
Mo1−S21	2.439(2)	Mo2−S61	2.429(2)
Mo1−S22	2.490(2)	Mo2−S62	2.486(2)
Mo1−S31	2.465(2)	Mo2−S41	2.468(2)
Mo1−S32	2.523(2)	Mo2−S42	2.522(2)
Mo1−S61	2.495(2)	Mo2−S21	2.491(2)
Mo1−Mo2	2.8462(8)		
S11−Mo1−S12	68.32(5)	S51−Mo2−S52	68.21(6)
S11−Mo1−S21	148.39(6)	S51−Mo2−S61	145.74(6)
S11−Mo1−S22	140.87(6)	S51−Mo2−S62	143.20(6)
S11−Mo1−S31	92.01(6)	S51−Mo2−S41	91.15(6)
S11−Mo1−S32	75.62(5)	S51−Mo2−S42	73.38(6)
S11−Mo1−S61	80.45(6)	S51−Mo2−S21	80.94(6)
S12−Mo1−S21	142.65(6)	S52−Mo2−S61	145.29(6)
S12−Mo1−S22	72.61(6)	S52−Mo2−S62	75.04(6)
S12−Mo1−S31	84.65(6)	S52−Mo2−S41	84.46(6)
S12−Mo1−S32	134.47(6)	S52−Mo2−S42	132.84(6)
S12−Mo1−S61	83.09(6)	S52−Mo2−S21	82.47(6)
S21−Mo1−S22	70.63(6)	S61−Mo2−S62	70.94(6)
S21−Mo1−S31	86.76(6)	S61−Mo2−S41	87.22(6)
S21−Mo1−S32	74.40(5)	S61−Mo2−S42	73.98(5)
S21−Mo1−S61	105.02(6)	S61−Mo2−S21	105.47(6)
S22−Mo1−S31	86.51(6)	S62−Mo2−S41	87.17(6)
S22−Mo1−S32	138.36(6)	S62−Mo2−S42	138.64(6)
S22−Mo1−S61	92.91(6)	S62−Mo2−S21	92.63(6)
S31−Mo1−S32	69.48(5)	S41−Mo2−S42	69.79(6)
S31−Mo1−S61	167.32(6)	S41−Mo2−S21	166.52(6)
S32−Mo1−S61	117.74(6)	S42−Mo2−S21	117.59(6)
Mo1−S21−Mo2	70.52(5)	Mo1−S61−Mo2	70.61(5)

which were related by a translation of half a unit cell along the *a* axis. These two molecules were essentially identical except for the conformation of one ethyl group, the orientation of the triflate counterion, and slight differences in the conformation of the PMe_2Ph ligand. Final full-matrix least-squares refinement of F^2 converged at R = 0.0511 for 11 237 reflections with $F_o > 4\sigma(F_o)$ and R = 0.0838 for all 17 026 unique reflections (wR_2 = 0.1149, 0.1378, respectively).

Kinetic Studies. UV−visible data were collected on a Beckman DU-7500 diode-array spectrophotometer equipped with a multicell transport block. The temperature was regulated by a thermostated water/ethylene glycol mixture circulated through the cell block and was measured by a thermocouple inserted in the cell block. Reactions of **4a** were carried out anaerobically in dichloromethane at 25.3 °C using 1 cm quartz cells fitted with septum caps and were monitored at 790 nm. Added reagents were present in >20-fold excess over **4a**, whose concentration was in the range $(2-4) \times 10^{-4}$ M. Three replicates were run for each set of experimental conditions. Pseudo-first-order rate constants were obtained for the halide substitution reactions using a least-squares fit to the equation $\ln|A_\infty - A| = -kt + \ln|A_\infty - A_0|$. The plots were linear for at least 4 half-lives.

Table 3. Selected Bond Lengths (Å) and Angles (deg) for $[Mo(PMe_2Ph)(S_2CNEt_2)_3](OTf)$ (**6**)

molecule 1		molecule 2	
Mo1−S11	2.4914(11)	Mo2−S21	2.4990(11)
Mo1−S12	2.4946(11)	Mo2−S22	2.4849(11)
Mo1−S13	2.4956(11)	Mo2−S23	2.4811(10)
Mo1−S14	2.4842(11)	Mo2−S24	2.4896(11)
Mo1−S15	2.5035(11)	Mo2−S25	2.5060(11)
Mo1−S16	2.4846(12)	Mo2−S26	2.4851(11)
Mo1−P1	2.5564(12)	Mo2−P2	2.5430(12)
S11−Mo1−S12	69.06(4)	S21−Mo2−S22	68.80(3)
S11−Mo1−S13	143.10(4)	S21−Mo2−S23	141.54(4)
S11−Mo1−S14	147.56(4)	S21−Mo2−S24	149.13(4)
S11−Mo1−S15	74.03(3)	S21−Mo2−S25	74.84(3)
S11−Mo1−S16	87.68(4)	S21−Mo2−S26	88.48(4)
S11−Mo1−P1	88.81(4)	S21−Mo2−P2	85.76(4)
S12−Mo1−S13	74.31(4)	S22−Mo2−S23	72.79(3)
S12−Mo1−S14	141.88(4)	S22−Mo2−S24	141.26(4)
S12−Mo1−S15	142.14(4)	S22−Mo2−S25	142.12(4)
S12−Mo1−S16	99.17(4)	S22−Mo2−S26	97.29(4)
S12−Mo1−P1	86.17(4)	S22−Mo2−P2	91.02(4)
S13−Mo1−S14	69.18(3)	S23−Mo2−S24	69.14(3)
S13−Mo1−S15	140.86(4)	S23−Mo2−S25	141.96(4)
S13−Mo1−S16	93.96(4)	S23−Mo2−S26	94.54(4)
S13−Mo1−P1	93.11(4)	S23−Mo2−P2	96.91(4)
S14−Mo1−S15	75.97(4)	S24−Mo2−S25	76.39(3)
S14−Mo1−S16	93.96(4)	S24−Mo2−S26	92.63(4)
S14−Mo1−P1	85.22(4)	S24−Mo2−P2	86.66(4)
S15−Mo1−S16	70.84(4)	S25−Mo2−S26	71.04(4)
S15−Mo1−P1	101.37(4)	S25−Mo2−P2	96.65(4)
S16−Mo1−P1	172.09(4)	S26−Mo2−P2	167.45(4)

Results

Synthesis and Characterization of $[Mo_2(S_2CNR_2)_6](OTf)_2$. The well-known Mo(VI) compounds $MoO_2(S_2CNR_2)_2$ [R = Et (**a** series), Me (**b** series)][8] provide a convenient entry into molybdenum(IV) tris(dithiocarbamate) complexes $MoX(S_2CNR_2)_3$ using a two-step route described by Chatt and coworkers (eqs 1 and 2).[5] The orange, air-stable, diamagnetic

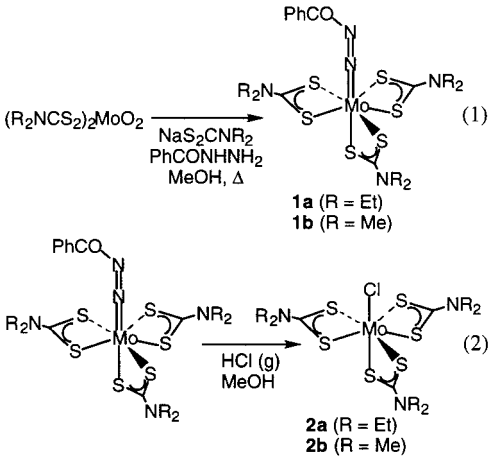

diazenido complexes $Mo(N_2COPh)(S_2CNR_2)_3$ (**1**) have C_s symmetry on the NMR time scale. This is consistent with the

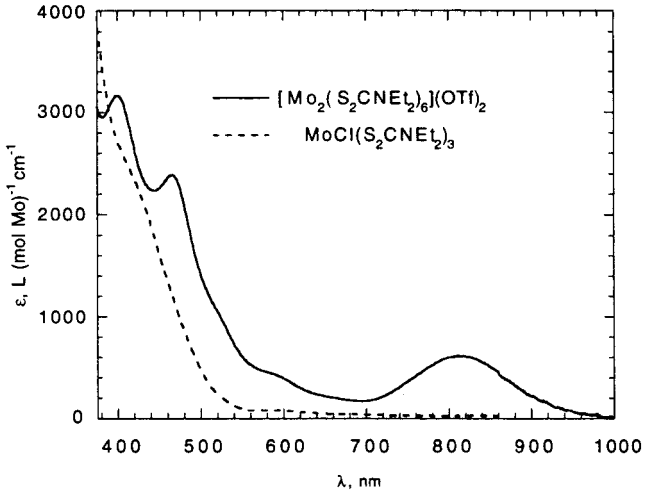

Figure 1. Optical spectra of $(Et_2NCS_2)_3MoCl$ (**2a**, dashed line) and $[Mo_2(S_2CNEt_2)_6](OTf)_2$ (**4a**, solid line) in CH_2Cl_2. Extinction coefficients are given per mole of Mo.

solid-state structures of the analogous complexes $Mo(N_2Ar)(S_2CNMe_2)_3$ (Ar = Ph, 3-$NO_2C_6H_4$)[10] and $Mo(N_2CO_2Et)(S_2CNMe_2)_3$,[11] which have a pentagonal bipyramidal geometry with apical diazenido ligands. The forest green, slightly air-sensitive chloro complexes $MoCl(S_2CNR_2)_3$, in contrast, show only a single set of alkyl resonances in their ^1H NMR spectra, with the hydrogens on the carbons directly attached to nitrogen appearing far downfield (δ 25.29 for the CH_2 resonance of **2a**, δ 38.41 for **2b** in CD_2Cl_2). This indicates that the seven-coordinate, 16-electron complexes are paramagnetic and undergo a rapid fluxional process that renders all alkyl groups equivalent at room temperature.

The chloride complexes **2** react rapidly in dichloromethane with silver trifluoromethanesulfonate (silver triflate, AgOTf) to precipitate AgCl and give air-sensitive species **4** of empirical formula $(R_2NCS_2)_3Mo(OTf)$ which are soluble in polar organic solvents such as acetone, CH_2Cl_2, $CHCl_3$, and CH_3CN and insoluble in ether, benzene, and hexane. The spectroscopic properties of the triflates **4** differ dramatically from those of the precursor chloride complexes **2**, suggesting that the reaction is not a simple metathesis of triflate for chloride. For example, the chloride complex **2a** is pale green, appearing yellow in dilute solution; its optical spectrum (Figure 1) shows a very weak band at 592 nm in addition to intense charge-transfer bands in the near-UV. The dark brown **4a** has a complex optical spectrum (Figure 1) and, in particular, shows a moderately intense (ϵ = 1200 M^{-1} cm^{-1}) absorption at rather long wavelengths (λ_{max} = 817 nm). The triflate complexes **4** exhibit ^1H and ^{13}C NMR spectra with dithiocarbamato resonances at normal chemical shifts and are therefore diamagnetic, in contrast to paramagnetic **2**. Furthermore, the NMR spectra of **4** show *six* inequivalent alkyl groups. For example, the spectrum of the dimethyldithiocarbamato analogue **4b** in acetone-d_6 shows six singlets of equal intensity and the methylene protons of **4a** are diastereotopic. Such a low-symmetry spectrum rules out a simple ionic formulation as $[Mo(S_2CNR_2)_3]OTf$, although the IR spectrum does show bands characteristic of ionic triflate.[12]

A solution to the structural conundrum is suggested by the FABMS of **4**, which show prominent peaks at masses corresponding to $Mo_2(S_2CNR_2)_6$. The dimeric structure of **4a** was

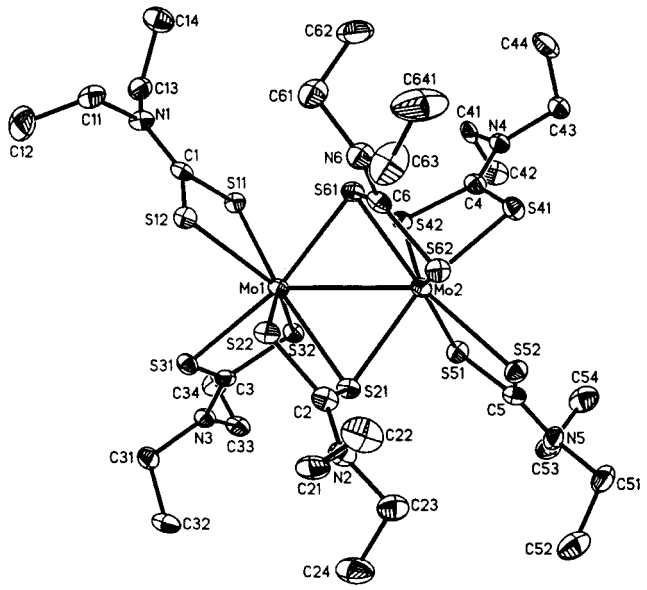

Figure 2. SHELXTL plot (30% thermal ellipsoids) of the cation of $[Mo_2(S_2CNEt_2)_6](OTf)_2{\cdot}4CHCl_3$ (**4a**·$4CHCl_3$).

confirmed by X-ray crystallography (Figure 2). Each $[Mo(S_2CNEt_2)_3]^+$ fragment forms a pentagonal bipyramidal structure with one apical group missing. One of the equatorial sulfur atoms on each $[Mo(S_2CNEt_2)_3]^+$ fragment (S21 on Mo1 and S61 on Mo2) binds to the vacant axial position on the other molybdenum. The bridging dithiocarbamates are both on the same face of the Mo_2S_2 core, giving the structure overall (noncrystallographic) C_2 symmetry. This mode of bridging is typical of edge-sharing bioctahedral complexes linked by bridging dithiocarbamates.[13] Dimeric **4** consists of two pentagonal bipyramids sharing an axial edge, a motif which has been seen before only once, in the osmium analogue $[Os_2(S_2CNEt_2)_6](PF_6)_2$ (**4$_{Os}$**).[14] Indeed, the molybdenum and osmium structures are remarkably similar on their peripheries, apart from the generally shorter bonds to osmium ($Os-S_{avg}$ = 2.415 Å in **4$_{Os}$** vs $Mo-S_{avg}$ = 2.492 Å in **4a**). However, the cores are significantly different because the molybdenum atoms in **4a**, at 2.8462(8) Å, approach each other much more closely than do the osmium atoms in **4$_{Os}$** [3.682(1) Å] or than the molybdenum atoms in dithiocarbamate-bridged $Mo_2(CO)_4(NO)_2(\mu\text{-}S_2CNEt_2)_2$ [3.773(1) Å].[15] The short Mo−Mo distance in **4a** induces very acute angles at the bridging sulfur atoms (70.56° vs 98.4° in **4$_{Os}$**) and clearly indicates a significant amount of Mo−Mo bonding. Spectroscopic and chemical evidence leave little doubt that the dimeric structure of **4** is retained in solution. For example, the optical spectrum of **4a** is quite different from monomeric Mo(IV) complexes, even at submillimolar concentrations. The NMR spectra that show six different alkyl groups for the dithiocarbamate ligands in **4** indicate that not only is the integrity of the dimer retained on the NMR time scale but that the structure is also nonfluxional. Both of these observations contrast starkly with the behavior of the osmium analogue **4$_{Os}$**, which shows only a single ethyl peak and is significantly

(10) Williams, G. A.; Smith, A. R. P. *Aust. J. Chem.* **1980**, *33*, 717−728.
(11) Butler, G.; Chatt, J.; Hussain, W.; Leigh, G. J.; Hughes, D. L. *Inorg. Chim. Acta* **1978**, *30*, L287−L288.
(12) Lawrance, G. A. *Chem. Rev.* **1986**, *86*, 17−33.
(13) (a) Raston, C. L.; White, A. H. *J. Chem. Soc., Dalton Trans.* **1975**, 2418−2425. (b) Mattson, B. M.; Heiman, J. R.; Pignolet, L. H. *Inorg. Chem.* **1976**, *15*, 564−571. (c) Landgrafe, C.; Sheldrick, W. S. *J. Chem. Soc., Dalton Trans.* **1994**, 1885−1893. (d) Abram, U. *Z. Anorg. Allg. Chem.* **1999**, *625*, 839−841. (e) Heard, P. J.; Kite, K.; Nielsen, J. S.; Tocher, D. A. *J. Chem. Soc., Dalton Trans.* **2000**, 1349−1356.
(14) Wheeler, S. H.; Pignolet, L. H. *Inorg. Chem.* **1980**, *19*, 972−979.
(15) Shiu, K.-B.; Lin, S.-T.; Fung, D. W.; Chan, T.-J.; Peng, S.-M.; Cheng, M.-C.; Chou, J. L. *Inorg. Chem.* **1995**, *34*, 854−863.

dissociated into paramagnetic monomers even at concentrations greater than 10 mM (although the dissociation is slow on the NMR time scale).[14] In the molybdenum complexes, the integrity of the dimers appears to persist at least for an hour or so in solution. When solutions of the diethyldithiocarbamate dimer **4a** and the dimethyldithiocarbamate dimer **4b** are mixed in acetone-d_6, the spectrum initially shows signals only for **4a,b** and undergoes spectral changes (possibly indicating some formation of a mixed ethyl/methyl dimer) only after several hours at room temperature.

Reactivity of $[Mo_2(S_2CNEt_2)_6](OTf)_2$. The dimeric complex **4a** reacts with a variety of donor ligands and oxidizing agents to form monomeric, pentagonal bipyramidal complexes of molybdenum(IV) or -(VI). For example, $[Ph_3P{=}N{=}PPh_3]Cl$ and $[Bu_4N]I$ react readily and quantitatively over the course of about 1 h in dichloromethane to give the halide complexes $MoCl(S_2CNEt_2)_3$ (**2a)** and $MoI(S_2CNEt_2)_3$, respectively. Sodium azide in acetonitrile reacts more slowly than the halides (~60% reacted after 24 h at room temperature), possibly because of the low solubility of NaN_3 in this solvent. The species that forms in this case has a broad dithiocarbamato methyl hydrogen resonance (δ 1.52) and paramagnetically shifted methylene hydrogens (δ 17.71). This species is assigned as the fluxional, 16-electron azido complex $Mo(N_3)(S_2CNEt_2)_3$ analogous to the halide complexes. Heating this complex in situ to 60 °C for 1 h completes the conversion of the azide to the nitrido complex **3a** (eq 3), which is present in only trace amounts after 24 h at room temperature. This is reminiscent of the literature preparation of **3** from the chloro complexes **2** and NaN_3 in refluxing methanol.[6]

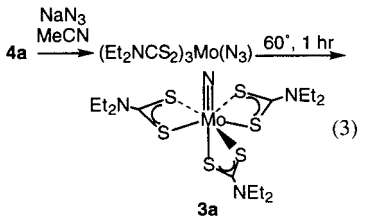

(3)

The molybdenum(IV) dimer $[Mo_2(S_2CNEt_2)_6](OTf)_2$ also reacts with a variety of neutral donors to form paramagnetic, fluxional adducts. For example, **4a** reacts quantitatively in acetone with PMe_2Ph within 2.5 h to form the phosphine adduct $[Mo(PMe_2Ph)(S_2CNEt_2)_3]OTf$ (**6**). PPh_3 reacts to form a similar adduct over the course of 1 day. The PCH_3 signals of **6** appear upfield in the ^{1}H NMR at δ −18.15, while the phenyl resonances are shifted downfield, as are the methylene protons of the dithiocarbamate ligands, appearing as a single peak at δ 35.39 ppm. The phosphine adduct **6** is soluble in chlorinated organic solvents and is insoluble in ether, hexane, and benzene.

The structure of **6**, as determined by X-ray diffraction, is shown in Figure 3. The two crystallographically independent cations, which differ only in the conformation of one ethyl group and the orientation of the PMe_2Ph ligand, adopt a pentagonal bipyramidal structure, as is invariably seen for seven-coordinate molybdenum tris(dithiocarbamato) complexes. The S_{ax}−Mo−P angles (170° average) are essentially linear. The Mo−S_{ax} bond distances (2.485 Å) are normal, indicating that the phosphine exerts a negligible trans influence.

Harder neutral donors also react with **4a** to form paramagnetic, fluxional monomers, albeit less favorably than do phosphines. For example, only 75% conversion to $[Mo(NCCD_3)(S_2CNEt_2)_3]OTf$ is seen even after 20 h in neat CD_3CN. No complexation is observed in neat acetone or with water in acetone-d_6. The triflate complex is sensitive to oxygen, turning

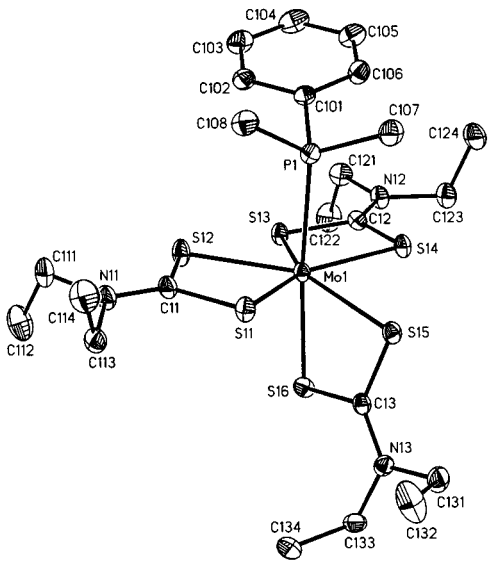

Figure 3. SHELXTL plot (30% thermal ellipsoids) of one of the two crystallographically independent cations in $[Mo(PMe_2Ph)(S_2CNEt_2)_3]$-OTf (**6**).

orange over several hours on exposure to air and forming diamagnetic $[MoO(S_2CNEt_2)_3]^+$.[16]

An exception to the generally slow rate of ligand substitution reactions of **4a** is its reaction with the nitrido complex **3a**, which rapidly (<5 min) cleaves the dimer in acetone-d_6 or CD_2Cl_2 to form an equilibrium mixture which contains the starting materials and a μ-nitrido dimer $[(Et_2NCS_2)_3Mo(\mu\text{-}N)Mo(S_2CN\text{-}Et_2)_3]OTf$ (**5a**), as characterized by NMR and FABMS (eq 4). The ^{1}H NMR spectrum of **5a** shows a single resonance at δ 17.94 for the dithiocarbamato methylene protons, indicating that

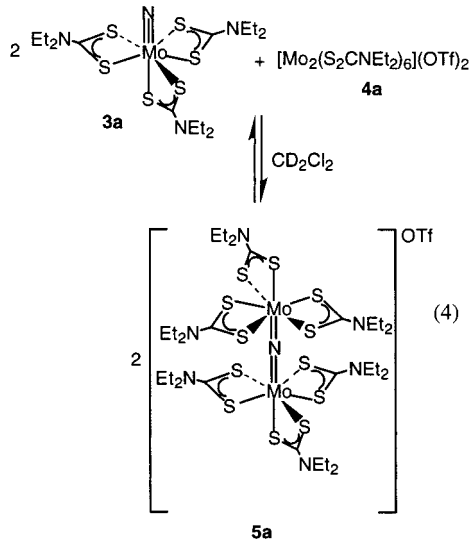

(4)

the $Mo(S_2CNEt_2)_3$ units are fluxional and that the cation is symmetrical on the NMR time scale. The equilibrium constant for eq 4 has been determined by NMR at several concentrations at 25 °C (eq 5).

$$K_4 = \frac{[\mathbf{5a}]^2}{[\mathbf{3a}]^2[\mathbf{4a}]} = 26 \pm 4\ \mathrm{M}^{-1} \qquad (5)$$

(16) Young, C. G.; Broomhead, J. A.; Boreham, C. J. *J. Chem. Soc., Dalton Trans.* **1983**, 2135−2138.

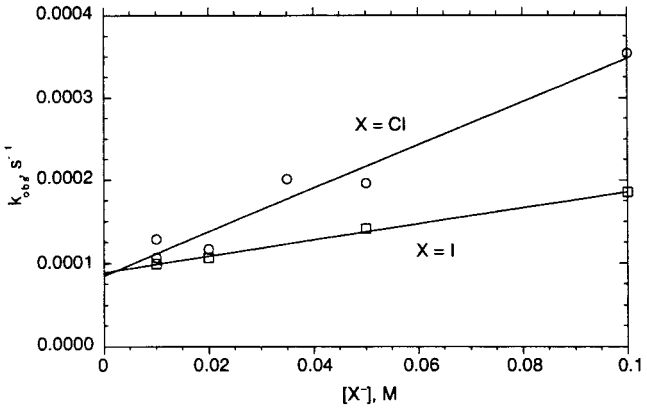

Figure 4. Observed pseudo-first-order rate constants for cleavage of [**4a**](OTf)$_2$ by $[Ph_3P{=}N{=}PPh_3]Cl$ or $[Bu_4N]I$ in the presence of $[Bu_4N]PF_6$ as a function of halide concentration. The total salt concentration is 0.1 M for all runs (CH_2Cl_2, 25.3 °C).

A reaction analogous to eq 4 occurs with the dimethyldithiocarbamato complexes **3b** and **4b** to form a Me_2NCS_2-ligated dimer (**5b**). Cross reactions also occur; thus **3a** and **4b**, or **3b** and **4a**, will react to form **5a,b** and the mixed dimer $[(Me_2NCS_2)_3Mo(\mu\text{-}N)Mo(S_2CNEt_2)_3]OTf$ (**5c**). The ^1H NMR of the mixed species shows a broad methyl resonance at δ 1.52 and paramagnetically shifted methyl and methylene resonances at δ 26.29 and 18.90, respectively.

Kinetics of Cleavage of 4a. The rates of ligand substitution of **4a** were examined using UV−visible spectroscopy in dichloromethane at 25.3 °C by monitoring the decrease in absorbance of **4a** at 790 nm. In the presence of both iodide and chloride (in excess), **4a** undergoes clean first-order decay to the corresponding monomeric halide complexes. There is no sign of intermediates in this reaction by NMR or UV−visible spectroscopy (for example, the **4a** → **2a** transformation is accompanied by an isosbestic point at 384 nm). If the total concentration of salts is kept constant using $[Bu_4N]PF_6$ as an inert electrolyte, the observed rate constants increase linearly with increasing concentration of halide for both chloride and iodide (Figure 4). A nonzero intercept is observed, which is the same within experimental error for both halides [$(8.4 \pm 1.3) \times 10^{-5}$ s^{-1} for Cl^-; $(8.9 \pm 0.3) \times 10^{-5}$ s^{-1} for I^-; total salt concentration of 0.1 M]. If the reaction is studied as a function of concentration of halide without adding electrolyte to maintain the salt concentration, however, there is only a slight dependence of the observed rate constant on halide concentration. The observed rate constants actually decrease somewhat with increasing chloride concentration in the absence of added electrolyte, ranging from a high of $5.22(10) \times 10^{-4}$ s^{-1} at 0.016 M [PPN]Cl and leveling off at $\sim 3.7 \times 10^{-4}$ s^{-1} [PPN]Cl concentrations over 0.05 M (Supporting Information, Figure S1). This pattern of ligand substitution rates that are linearly dependent on concentration of entering ligand at constant salt concentration but insensitive to ligand concentration in the absence of inert salt has been observed previously in ligand substitution reactions of cationic metal complexes with anionic ligands.[17,18] It is most consistent with substitution taking place within contact ion pairs, as expected in nonpolar dichloromethane, where adding chloride cannot increase the concentration of the ion pair, but inert electrolyte can decrease the fraction of reactive anion in the ion pairs.[19]

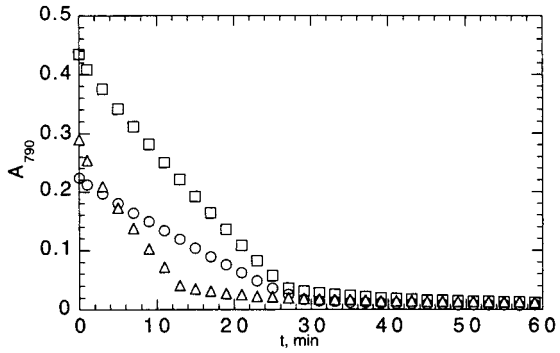

Figure 5. Kinetics of ligand substitution of **4a** by PMe_2Ph in CH_2Cl_2 at 25.3 °C. Reaction conditions are the following: (a) [**4a**] = 0.2 mM, [PMe_2Ph] = 17.4 mM (solid squares); (b) [**4a**] = 0.1 mM, [PMe_2Ph] = 17.4 mM (open squares); (c) [**4a**] = 0.13 mM, [PMe_2Ph] = 102.8 mM (solid triangles).

Analogous studies with the neutral ligand PMe_2Ph give qualitatively different results. Again, NMR and UV−vis data suggest a clean **4a** → **6** transformation (e.g., an isosbestic point is observed at 441 nm). However, reactions with a large excess of PMe_2Ph do *not* show first-order decay of **4a**, instead reproducibly giving absorbance vs time profiles as shown in Figure 5. The plots show a linear decay accounting for ~85% of the reaction, followed by a decelerating phase. The slope of the "pseudo-zero-order" phase is proportional to the **4a** concentration (compare runs a and b in Figure 5). There is no induction period; if anything, the reaction shows a very slight deceleration before entering the linear phase. It appears unlikely that this behavior is due to the presence of adventitious impurities in **4a**, since different batches of the dimer, prepared by halide abstraction using AgOTf or TlOTf, give identical results. Similar behavior is seen when acetone is used as solvent rather than dichloromethane.

Discussion

Bonding in $[Mo_2(S_2CNR_2)_6](OTf)_2$ (4). The monomeric, paramagnetic molybdenum tris(dithiocarbamato) chloride complexes **2**[5] undergo facile halide abstraction with silver or thallium triflate. The products of halide abstraction are not monomeric cations or triflate complexes but rather the diamagnetic dimers $[Mo_2(S_2CNR_2)_6](OTf)_2$ (**4**), where the axial site vacated by halide has been filled by a bridging sulfur atom from an equatorial dithiocarbamate ligand of another molybdenum center. The structures of **4**, as illustrated by the solid-state structure of **4a** (Figure 2), consist of two molybdenum atoms each surrounded by a roughly pentagonal bipyramidal array of sulfur atoms, with the two coordination polyhedra sharing an axial edge.

The gross structure of **4a** is strikingly similar to that of the dicationic osmium analogue $[Os_2(S_2CNEt_2)_6](PF_6)_2$ ($\mathbf{4_{Os}}$) described by Wheeler and Pignolet.[14] Only one major discrepancy mars the remarkable agreement between the two structures, namely the metal−metal separation, which is clearly nonbonding in $\mathbf{4_{Os}}$ [Os−Os = 3.682(1) Å] and clearly bonding in **4a** [Mo−Mo = 2.8462(8)]. The chemistry of the molybdenum dimer also shows that it has greater cohesion than its osmium analogue. $\mathbf{4_{Os}}$ is fluxional on the NMR time scale, in equilibrium with detectable amounts of monomeric $[Os(S_2CNEt_2)_3]^+$, and reacts rapidly and completely with donor solvents such as CH_3CN to

(17) (a) Romeo, R.; Arena, G.; Scolaro, L. M.; Plutino, M. R. *Inorg. Chim. Acta* **1995**, *240*, 81−92. (b) Alibrandi, G.; Romeo, R.; Scolaro, L. M.; Tobe, M. L. *Inorg. Chem.* **1992**, *31*, 5061−5066.
(18) Song, L.; Trogler, W. C. *J. Am. Chem. Soc.* **1992**, *114*, 3355−3361.
(19) Loupy, A.; Tchoubar, B.; Astruc, D. *Chem. Rev.* **1992**, *92*, 1141−1165.

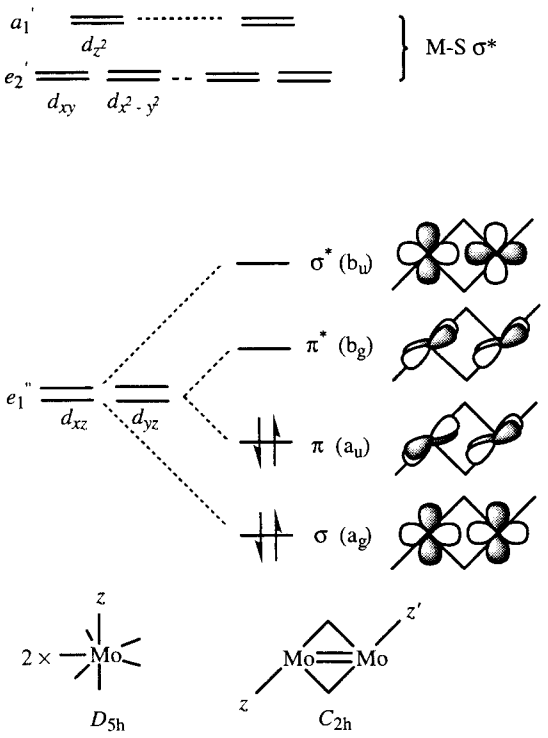

Figure 6. Qualitative molecular orbital diagram for $[Mo_2(S_2CNR_2)_6](OTf)_2$ (**4**). Nonbridging equatorial ligands in **4** are omitted for clarity.

form monomeric seven-coordinate adducts.[14] The molybdenum dimer **4a** shows six inequivalent alkyl groups on the NMR time scale, shows no tendency to form monomers in noncoordinating solvents, and forms monomeric adducts only slowly and incompletely in acetonitrile. Thus, the molybdenum−molybdenum bond in **4a** appears to have both structural and chemical consequences. It is not obvious, however, why **4a** should be diamagnetic, since the Mo−Mo separation in the d^2-d^2 dimer is typical of a single bond[20] and is almost 0.05 Å longer than the longest double bond length we are aware of in a symmetrical[21] dimolybdenum complex, 2.798 Å in $(MeCp)_2Mo_2(CO)_4(\mu$-fluorenylidene).[22] Although the bond length/bond order correlation must be treated with considerable caution,[7] the extreme length of the bond seemed to merit more careful analysis.

The qualitative molecular orbital diagram illustrated in Figure 6 clarifies the initially puzzling aspects of the bonding of **4a**. If one first considers the metal−ligand interactions in each pentagonal bipyramidal (PBP) Mo fragment (idealized D_{5h} symmetry), the orbitals split into a set of three with Mo−S σ^* character (d_{xy}, $d_{x^2-y^2}$, d_{z^2}) and a degenerate pair that are π with respect to the ligands (d_{xz}, d_{yz}). Tipping the axes of the two PBP Mo fragments allows their assembly into the edge-shared dimer (center of Figure 6). If the reasonable assumption is made that the metal−sulfur interaction is much stronger than the metal−metal interaction, then the energy gap between the orbitals will be large and the mixing between them small, and only the Mo−S nonbonding e_2'' orbitals of the PBP Mo fragments need to be considered (to a first approximation) in the description of the metal−metal bonding.

The molybdenum(IV) dimers **4** have only C_2 symmetry, but if the chelation of the dithiocarbamates is ignored, then the Mo_2S_{12} core has nearly C_{2h} symmetry, with the σ_h plane defined by the Mo_2S_2 core. Two of the Mo−S nonbonding orbitals interact in a σ fashion, which creates the Mo1−Mo2 σ bonding and antibonding orbitals of a_g and b_u symmetry. The other two orbitals produce another bonding/antibonding pair, of a_u and b_g symmetry, respectively (Figure 6). The latter pair are nominally of π symmetry, but because of the constraints of the PBP ligand framework, the orbitals are roughly parallel to each other rather than pointed at each other. This "skewed-π" interaction could equally well be described as a sort of slipped δ bond. A δ interaction would normally be expected to be negligible at 2.85 Å, but the skewing of the orbitals toward each other is expected to increase their overlap, perhaps enough to resemble that seen in a more typical δ bond in a complex with a much shorter metal−metal separation. A very similar bonding scheme was suggested for $Mo_2(O^iPr)_8$, which consists of two trigonal bipyramids sharing an axial edge.[23] The much shorter Mo−Mo bond in $Mo_2(O^iPr)_8$ (2.523 Å) than in **4a** is probably largely due to differences in the bridging ligands (compare the nonbonded Mo−Mo distance of 3.335 Å in $Mo_2(NO)_2(O^iPr)_4(\mu$-$O^iPr)_2$[24] with that of 3.773 Å in $Mo_2(CO)_4(NO)_2(\mu$-$S_2CNEt_2)_2$[15]).

The analogy with δ bonding is strongly supported by the optical spectrum of **4a** (Figure 1). In particular, the lowest energy band, at 817 nm (12 200 cm^{-1}), is assigned to the $a_u \rightarrow b_g$ transition. The modest intensity of this dipole-allowed band ($\epsilon = 1200\ M^{-1}\ cm^{-1}$) is reminiscent of the low intensities typical of $\delta \rightarrow \delta^*$ transitions in metal−metal quadruply bonded dimers, where the nominally allowed transitions are quite weak by virtue of the small overlap between the metal d orbitals.[25] The complex optical spectrum of **4a**, with multiple shoulders in the 500−800 nm range and two strong bands at higher energy, also appears to be qualitatively consistent with this four-orbital picture.

In short, the bonding in dimeric **4** appears to be well-described as a metal−metal double bond consisting of a reasonably strong σ bond and a rather weak δ-like "skewed-π" bond. The latter interaction splits the a_u and b_g orbitals enough to pair the electrons and render the complex diamagnetic but is expected to contribute only slightly to the metal−metal attraction. Hence, the double bond is quite long, with a distance more typical of a molybdenum−molybdenum single bond.

Mechanism of Ligand Substitution in $[Mo_2(S_2CNEt_2)_6](OTf)_2$. Given the presence of a metal−metal bond in **4**, it was not obvious whether these dimeric complexes would serve as useful sources of the $\{Mo(S_2CNR_2)_3\}^+$ fragment. In fact, addition of ligands and formation of seven-coordinate monomers from **4a** takes place readily with a variety of reagents, including halides, phosphines, azide (ultimately forming the terminal nitride complex **3a**), and oxygen (forming a Mo(VI) oxo complex). Qualitatively, rates span a considerable range, with reaction of **4a** with $MoN(S_2CNEt_2)_3$ (**3a**) coming to equilibrium

(20) Cotton, F. A. *J. Less-Common Met.* **1977**, *54*, 3−12.
(21) Longer Mo−Mo distances (up to 2.94 Å) have been assigned as double bonds in *unsymmetrical* phosphido-bridged dimolybdenum complexes on the basis of simple electron-counting considerations, but the asymmetry in these complexes also allows their formulation as having a single bond with a pair of electrons in a localized nonbonding orbital. (a) Endrich, K.; Korswagen, R.; Zahn, T.; Ziegler, M. L. *Angew. Chem., Int. Ed. Engl.* **1982**, *21*, 919. (b) Adatia, T.; McPartlin, M.; Mays, M. J.; Morris, M. J.; Raithby, P. R. *J. Chem. Soc., Dalton Trans.* **1989**, 1555−1564. (c) Conole, G.; McPartlin, M.; Mays, M. J.; Morris, M. J. *J. Chem. Soc., Dalton Trans.* **1990**, 2359−2366. (d) Adams, H.; Bailey, N. A.; Hempstead, P. D.; Morris, M. J.; Riley, S.; Beddoes, R. L.; Cook, E. S. *J. Chem. Soc., Dalton Trans.* **1993**, 91−100. (e) Stichbury, J. C.; Mays, M. J.; Davies, J. E.; Raithby, P. R.; Shields, G. P.; Finch, A. G. *Inorg. Chim. Acta* **1997**, *262*, 9−20.
(22) Curtis, M. D.; Messerle, L.; D'Errico, J. J.; Solis, H. E.; Barcelo, I. D.; Butler, W. M. *J. Am. Chem. Soc.* **1987**, *109*, 3603−3616.
(23) Chisholm, M. H.; Cotton, F. A.; Extine, M. W.; Reichert, W. W. *Inorg. Chem.* **1978**, *17*, 2944−2946.
(24) Chisholm, M. H.; Cotton, F. A.; Extine, M. W.; Kelly, R. L. *J. Am. Chem. Soc.* **1978**, *100*, 3354−3358.
(25) Trogler, W. C.; Gray, H. B. *Acc. Chem. Res.* **1978**, *11*, 232−239.

within minutes (eq 4), while equilibration with neat CD_3CN takes about 1 day.

The rates of reaction of **4a** with chloride and iodide ions are well-behaved and allow two important mechanistic conclusions to be drawn. First, the rate of reaction does not increase significantly with increasing overall chloride concentration (in the absence of other ions). This indicates that attack on $[Mo_2(S_2CNEt_2)_6]^{2+}$ by external chloride does not contribute significantly to the rate of the reaction; in other words, the chloride that is involved in the reaction is ion-paired with the molybdenum complex. This behavior appears to be typical of anionic nucleophiles reacting with cationic metal complexes in CH_2Cl_2.[17,18] If the total quantity of ions is fixed, the ligand substitution rate does increase linearly with increasing fraction of chloride or iodide. Reaction rates for both halides extrapolate to the same positive intercept at zero halide concentration. This suggests a two-term rate law in this reaction (eq 6) and hence two independent mechanisms for the reaction.

$$k = k_{diss} + k_X \frac{[X^-]}{[X^-] + [PF_6^-]} \qquad (6)$$

$$k_{diss} = 8.7(8) \times 10^{-5}\ s^{-1}$$

$$k_{Cl} = 2.6(3) \times 10^{-4}\ s^{-1}$$

$$k_I = 9.8(4) \times 10^{-5}\ s^{-1}$$

At low fraction of halide, a halide-independent mechanism predominates. This is most likely simple dissociation of $[Mo_2(S_2CNEt_2)_6]^{2+}$ into monomeric $[Mo(S_2CNEt_2)_3]^+$, although assistance by CH_2Cl_2 or PF_6^- in this dissociation cannot be ruled out. With increasing amounts of halide, attack by halide on the intact dimer becomes more important, with chloride reacting about three times more efficiently by this route than iodide. The linear dependence of rate on halide fraction indicates that addition of only one halide ion is sufficient to lead irreversibly to dimer scission.

The presence of an associative, as well as a dissociative, reaction pathway is consistent with the wide variation in rates of reaction of **4a** with nucleophiles. The ligands can be arranged qualitatively in order of decreasing rate of reaction with **4a** as follows:

$$(R_2NCS_2)_3MoN \gg Cl^- \approx PMe_2Ph > PPh_3 \gg CH_3CN$$

This ordering correlates roughly with ligand nucleophilicity, with the glaring exception of the molybdenum nitride **3**. Even though $(Et_2NCS_2)_3MoN$ (**3a**) is commonly described as one of the most nucleophilic nitrides known,[6,26] it is difficult to see how it could be more nucleophilic than PMe_2Ph in any simple displacement reaction. Certainly the kinetically facile reaction of **3** is not favored by a large thermodynamic driving force, as reaction of **3** with **4a** achieves a measurable equilibrium ($K_4 = 24\ M^{-1}$), while the much more slowly reacting phosphines form only adducts at equilibrium. Possibly the ability of the Mo(VI) nitride **3** to accept electrons from the Mo(IV) dimer **4** in forming the Mo(V)−Mo(V) product **5** may help to break up **4**, giving the nitride **3** a kinetic advantage over redox-inert ligands.

However, the puzzling kinetics of the reaction of **4a** with PMe_2Ph (Figure 5) should inject a note of caution into any discussion of the mechanism of reaction of **4a** with neutral donors. In these reactions, decay of **4a** is dominated by a linear phase which accounts for ~85% of the reaction and whose rate is proportional to the initial concentration of **4a**. While many other dimeric systems show zero-order kinetics in entering ligand or reagent,[27−30] in no case that we know of is the reaction zero-order in the metal complex! Indeed, no combination of rate constants in a general scheme for ligand-induced monomerization (such as that given by Espenson[31]) will give a rate law that is independent of [**4a**] over the course of the reaction. The reaction rates with PMe_2Ph do increase with increasing phosphine concentration, suggesting that this reaction is at least in part associative, but beyond that it is not at all clear what detailed mechanism is operating in this case.

Conclusions

Halide abstraction from $MoCl(S_2CNR_2)_3$ provides ready access to the new binuclear complexes $[Mo_2(S_2CNR_2)_6](OTf)_2$ (**4**). An X-ray structural study of **4a** (R = Et) reveals that the dimer possesses an unusual edge-shared pentagonal bipyramidal structure with a Mo_2S_2 core. The diamagnetism and optical spectra are most consistent with a Mo−Mo bond order of 2, though the Mo−Mo distance of 2.85 Å is more typical of Mo−Mo single bonds. This is rationalized by the description of the double bond as consisting of a normal σ bond and a weak "skewed π" bond similar to a normal δ bond. In its ligand substitution chemistry **4a** acts as a source of the $[Mo(S_2CNEt_2)_3]^+$ fragment; it reacts with azide to form $MoN(S_2CNEt_2)_3$ (**3a**) and with PMe_2Ph to form the new complex $[Mo(PMe_2Ph)(S_2CNEt_2)_3]OTf$ (**6**), which has been structurally characterized. **4a** can react by both associative and dissociative pathways. Associative pathways appear to be preferred, although the mechanisms can be complex and may vary with the nature of the incoming ligand.

Acknowledgment. We thank Dr. Alicia Beatty for her assistance with the X-ray structures, Prof. W. Robert Scheidt for the use of his near-IR spectrophotometer, and Prof. A. Graham Lappin for helpful discussions regarding the dimer cleavage kinetics. Support from the National Science Foundation (Grant CHE-97-33321-CAREER), the Camille and Henry Dreyfus Foundation (New Professor Award), DuPont (Young Professor Award), the Dow Chemical Co. (Innovation Recognition Program), and the Arthur J. Schmitt Foundation (fellowship to S.B.S.) is gratefully acknowledged.

Supporting Information Available: A figure showing the of variation of rates of chloride addition to **4a** as a function of total $[Cl^-]$, tables of crystallographic parameters, atomic coordinates, bond lengths and angles, anisotropic thermal parameters, hydrogen coordinates for **4a**·$4CHCl_3$ and **6**, and CIF data. This material is available free of charge via the Internet at http://pubs.acs.org.

IC010673Y

(26) Bishop, M. W.; Chatt, J.; Dilworth, J. R.; Neaves, B. D.; Dahlstrom, P.; Hyde, J.; Zubieta, J. *J. Organomet. Chem.* **1981**, *213*, 109−124.

(27) Orino, H.; Shimura, M.; Yamamoto, N.; Okubo, N. *Inorg. Chem.* **1988**, *27*, 172−175 and references therein.

(28) Wilson, L. M.; Cannon, R. D. *Inorg. Chem.* **1985**, *24*, 4366−4371.

(29) Fawcett, J. P.; Poe, A.; Sharma, K. R. *J. Am. Chem. Soc.* **1976**, *98*, 1401−1407.

(30) Deal, K. A.; Burstyn, J. N. *Inorg. Chem.* **1996**, *35*, 2792−2798.

(31) (a) Lente, G.; Guzei, I. A.; Espenson, J. H. *Inorg. Chem.* **2000**, *39*, 1311−1319. (b) Lente, G.; Jacob, J.; Guzei, I. A.; Espenson, J. H. *Inorg. React. Mech.* **2000**, *2*, 169−177.